NASA Contractor Report 165126

MICROSTRUCTURE AND MECHANICAL PROPERTIES OF BULK AND PLASMA-SPRAYED Y_2O_3-PARTIALLY STABILIZED ZIRCONIA

Peter G. Valentine and Ralph D. Maier

Case Western Reserve University
Cleveland, Ohio 44106

August 1980

Prepared for

NATIONAL AERONAUTICS AND SPACE ADMINISTRATION
Lewis Research Center
Under Grant NSG-3252

MICROSTRUCTURE AND MECHANICAL PROPERTIES OF BULK AND PLASMA-SPRAYED Y_2O_3-PARTIALLY STABILIZED ZIRCONIA

by

Peter G. Valentine and Ralph D. Maier

Case Western Reserve University
Cleveland, Ohio 44106

SUMMARY

A commercially available bulk 8.0 weight-percent yttria (Y_2O_3) partially stabilized zirconia (PSZ) was studied by light microscopy, transmission electron microscopy, X-ray analysis, microhardness testing, and fracture toughness testing. In the as-received condition this material exhibited 28μm equiaxed grains which were comprised of 0.06μm coherent tetragonal precipitates situated in a cross-hatch or tweed configuration in a cubic matrix. In addition, the PSZ contained larger spheroidal and grain boundary precipitates up to 4μm in size which were either metastable tetragonal or monoclinic in structure. Spheroids up to 1.26μm in diameter were tetragonal; large spheroids were monoclinic. These metastable tetragonal precipitates are the largest thus far reported for a PSZ system.

Solution annealing and air quenching the as-received PSZ eliminated the large precipitates, but fine tetragonal precipitates arranged in a cross-hatch pattern reformed during the air quench. Aging the as-received PSZ at 1500^0 C caused the fine tetragonal precipitates to grow from 0.06 to 0.12μm in 250 minutes. A peak hardness of about 1400 kg/mm^2 was attained after 50 minutes. The loss in strength which occurred on further aging was associated with the growth of the fine tetragonal precipitates.

Aging the solution-annealed-and-quenched PSZ caused the fine, 0.02μm, tetragonal precipitates to grow into plates approximately 0.10μm by 0.50μm in size. A peak hardness of 1517 kg/mm^2 was obtained after aging the PSZ for 250 minutes at 1500^0 C. With further aging monoclinic precipitates were found to form along the grain boundaries. These monoclinic precipitates are associated with the drop in hardness of the PSZ at long aging times.

Grinding the Y_2O_3-PSZ into a powder did not cause a significant amount of metastable tetragonal to transform to monoclinic in agreement with the prior work. This fact indicates that transformation toughening is not a significant mechanism in Y_2O_3-PSZ. The fracture toughness of the aged and unaged solution-annealed-and-quenched PSZ was found to be between 2 and 3 MN/m$^{3/2}$. This range of fracture toughness is consistent with PSZ's that do not undergo transformation toughening.

Introduction

Zirconia, ZrO_2, exhibiits three polymorphic crystal structures between room temperature and its melting temperature, which are as follows: (1) monoclinic, (2) tetragonal, and (3) cubic. The structure of ZrO_2 between room temperature and about 1100^0C is monoclinic. From about 1100^0C to 2370^0C, zirconia has a tetragonal structure. The high temperature polymorph, which is stable between 2370^0C and its melting temperature (approximately 2700^0C), has a cubic fluorite (CaF_2) structure.

A martensitic tetragonal-monoclinic transformation occurs when ZrO_2 is cooled from above 1100^0C. This transformation has been proven to be martensitic because it exhibits a thermal hysteresis, is characterized by a simple shape change caused by a cooperative shear, is diffusionless, and is reversible. When cooled from elevated temperatures (above 1100^0C) the material has a tendency to crack due to a volume expansion that takes place during the martensitic transformation. The use of pure zirconia has been greatly limited due to the fact that this cracking can be so severe that the ZrO_2 will actually disintegrate into powder during thermal cycling.

By alloying ZrO_2 with other oxides such as MgO, CaO, and Y_2O_3, the cubic phase can be retained at room temperature. The addition of these oxides to ZrO_2 lowers the cubic-to-tetragonal transition temperature below that of pure zirconia. The amount of oxide added to zirconia will determine whether the material will be entirely cubic (fully stabilized) or a two phase mixture of cubic phase and another phase (partially stabilized). The second phase, in the partially stabilized zirconia (PSZ), may be either equilibrium monoclinic precipitates or fine tetragonal pre-

cipitates or fine tetragonal precipitates retained metastably at room temperature by coherency strains. If the tetragonal precipitates are overaged, resulting in a loss of coherency, they will transform to a stable monoclinic phase.

Fully stabilized zirconia is resistant to the problems associated with the martensitic transformation, but its thermal shock resistance is still relatively poor due to a high thermal expansion coefficient and a low thermal diffusivity. The two-phase microstructure of partially stabilized zirconia provides the best combination of mechanical properties, although these properties have been found to vary significantly depending on the size and distribution of the second phase.

Recently, plasma-sprayed partially stabilized zirconia (PSZ) has demonstrated considerable potential as a thermal barrier coating for aircraft gas turbine blades (1-6). A preliminary study (7) of the plasma-sprayed material revealed a large range of structures within the coating depending on its local thermal history. The purpose of this work is to attain an improved understanding of the Y_2O_3-PSZ system and to apply this knowledge to plasma-sprayed thermal barrier coatings. The initial research has been performed with commercially available bulk material because it is more uniform in microstructure, composition, and thermal history than the plasma-sprayed material. This work will provide the fundamental background necessary to study the more complex plasma-sprayed coatings.

Materials and Procedure

A commercially available bulk 8.0 weight-percent yttria (Y_2O_3) partially stabilized zirconia (PSZ) was characterized in the as-received condition as well as after thermal treatments. Three types of thermal treatments were employed:

(1) as-received material was solution annealed and quenched,

(2) as-received material was aged for various times at 1500^0C, and

(3) solution-annealed material was aged for various times at 1500^0C.

Characterization was accomplished by standard techniques including light microscopy (LM), transmission electron microscopy (TEM), X-ray analysis, and microhardness testing. The fracture toughness was determined by the overloaded Vickers indentation technique (8).

Results and Discussion

The PSZ was produced by sintering powder into bulk form at an elevated temperature and then slowly cooling the material down to room temperature. The resultant microstructure, as revealed by LM, is comprised of 28μm grains which contain a small percentage of spheroidal precipitates a few microns in size, grain boundary precipitates, and some porosity as shown in Figure 1. TEM techniques revealed that the material consisted primarily of very fine coherent tetragonal precipitates in a cubic matrix. These metastable tetragonal precipitates do not transform to monoclinic because of coherency strains. The bright field TEM mode showed only the strain contrast caused by coherent precipitates (Figure 2a); the dark field mode, however, revealed

the 0.06μm tetragonal precipitates situated in a cross-hatch or tweed-like pattern (Figures 2b and 2c). These dark field images were produced using fluorite-forbidden reflections which arise only from the tetragonal and not from the cubic phase.

The TEM was also used to demonstrate that the spheroids and grain boundary precipitates were either metastable tetragonal or monoclinic in structure. The spheroidal particles ranged in size from 0.74μm to 3.50μm, and the grain boundary precipitates were as large as 3 to 4μm in length. The structures of the spheroids appeared to be related to their size. Smaller spheroids were tetragonal; larger shperoids were monoclinic. Tetragonal spheroids as large as 1.26μm were observed and appeared relatively featureless as shown in Figure 3. The larger spheroidal precipitates exhibited a monoclinic structure and the numerous twins which are associated with the tetragonal-to-monoclinic phase transformation. A twinned monoclinic spheroid, 3.50μm in diameter is presented in Figure 4a, and its selected area electron diffraction (SAD) pattern is shown in Figure 4b. It is noted that similar twinned spheroidal precipitates that also have undergone a martensitic transformation were reported for a Cu-1 weight percent Fe alloy (9). A grain boundary precipitate and the adjacent grain are shown in Figure 5. The grains exhibit strain contrast and the precipitate exhibits a few twin-like features which suggest that at least part of the precipitate has transformed from tetragonal to monoclinic.

The microstructure of the commercially produced Y_2O_3-PSZ can be explained with the aid of the Y_2O_3-ZrO_2 phase diagram presented in

Figure 6 which shows a vertical line at 4.5 mole-percent Y_2O_3 (8.0 wt.-% Y_2O_3) to represent the composition employed in this study. The microstructure suggests that the sintering operation was performed in the tetragonal + cubic two phase field at a temperature not far below the single phase cubic region. At this temperature cubic and a small percentage of tetragonal were in equilibrium. This temperature favored the formation of a few relatively large tetragonal precipitates which nucleated at energetically favorable sites, such as grain boundaries. On cooling through the two phase field, the equilibrium amount of tetragonal phase increased and numerous small coherent tetragonal particles were precipitated within the grains in a tweed configuration. On further cooling to room temperature some of the large tetragonal precipitates which had formed at the elevated sintering temperature transformed to equilibrium monoclinic and experienced considerable twinning. Spheroids 1.26μm or less in diameter did not undergo this transformation and remained as metastable tetragonal. It is noted that these spheroids are larger than any metastable tetragonal particles previously reported for PSZ systems (10-12). In particular, Gupta (12) working with a PSZ containing small amounts of Y_2O_3 found that metastable tetragonal grains could be retained at room temperature if the grain size was below 0.3μm.

A solution annealing treatment significantly modified the microstructure of the PSZ. The material was annealed in the single phase cubic region shown in Figure 6 and then air quenched to room temperature. The annealing treatment dissolved all of the second phase precipitates. LM revealed the absence of the large spheroidal and grain

boundary precipitates evident in the as-received material (Figure 7). In addition, grain growth at the annealing temperature caused the grain size to increase from 28 to 37μm. Bright-field TEM revealed only strain contrast similar to that observed for the as-received PSZ, as shown in Figure 8a. In the dark-field mode 0.02μm coherent tetragonal particles which precipitated during the air quench to room temperature were observed, as shown in Figure 8b. Note that the particles exhibit alignment in two directions, or a cross-hatch configuration. The microhardness of this material was measured to be 1376 kg/mm^2. This high hardness is attributed to the presence of the coherent tetragonal precipitates.

The influence of aging on the microstructure and microhardness of the as-received PSZ was also sutdied. The microhardness is presented as a function of aging time at 1500^0 C in Figure 9. The PSZ exhibits a typical precipitation hardening behavior, attaining a peak hardness of about 1400 kg/mm^2, after 50 minutes and decreasing in hardness with further aging. LM revealed that aging at 1500^0 C increased the grain size slowly from 28 to 30μm in 250 minutes. A low magnification dark-field TEM view of the specimen aged for 50 minutes revealed tetragonal precipitates in a tweed pattern (Figure 10). The bright-field mode showed only strain contrast. However, with increasing aging time the precipitates grew and the strain contrast, and therefore the strain in the material decreased, allowing improved imaging of the tetragonal precipitates. Bright and dark-field views of the precipitates in the material aged for 250 minutes at 1500^0 C are presented in Figure 11. Note that the fluorite-forbidden reflection

employed for the dark-field image illuminated only one tetragonal variant while the others remained dark. The tetragonal precipitates, which were 0.06μm in the as-received condition, were found to grow to 0.12μm after aging for 250 minutes at 1500^{0}C.

The solution-annealed material was also aged for various lengths of time at 1500^{0}C to permit the influence of aging time on microstructure and mechanical behavior to be established. The microhardness is presented as a function of aging time at 1500^{0}C in Figure 12. The microhardness curve for the as-received material is also shown in Figure 12 for the sake of comparison. The solution-annealed-and-quenched material reached a peak hardness of 1517 kg/mm^2 after four hours at 1500^{0}C and its hardness didn't diminish significantly until after three days at 1500^{0}C. The solution-annealed-and quenched material was found to require a longer time at 1500^{0}C to reach its peak hardness than the as-received material. Also, once the peak hardness was reached much longer times, than those required for the as-received material, were needed in order for the hardness to drop significantly. The aging behavior of the solution-annealed-and quenched PSZ is much more sluggish, and yields much better results, than that of partially stabilized zirconias that contain oxides other than Y_2O_3, such as MgO. For example, in a 8.1 mole-% MgO-PSZ (12) that was aged at 1400^{0}C a peak hardness of 1174 kg/mm^2 occurred after 30 minutes and upon further aging the hardness dropped rapidly to approximately 800 kg/mm^2. LM revealed that aging at 1500^{0}C increased the grain size from 37μm to 51μm in 10,080 minutes.

As noted above, the solution-annealed-and-quenched material contained 0.02μm coherent tetragonal particles aligned in <112> directions. After aging for 50 minutes at 1500°C, the coherent tetragonal particles had grown to 0.04μm in size and were observed to be aligned in <112> directions (Figure 13). Figure 8b and Figure 13, micrographs of the solution-annealed material and the solution-annealed material after aging for 50 minutes, respectively, were both taken after the specimens were tilted close to a $[\bar{1}11]$ zone.

Figure 14 is a micrograph of a typical $[\bar{1}11]$ zone found in the solution-annealed and aged specimens. In this figure arrows point out {220}, {112}, and {110} type spots. The {220} type reflections are due to the cubic matrix and to the tetragonal precipitates. The {112} type reflections are superlattice spots and are due to the three possible variants of the tetragonal phase, so that there are three sets (or pairs) of {112} type spots with a single pair of {112} spots being a particular {112} spot and the spot located directly opposite it from the transmitted or (000) spot. These three variants arise from the c-axis of the tetragonal unit cell being able to line up in any one of three mutually perpendicular directions (note: the a- and b-axes of the tetragonal unit cell are equal or equivalent). The other type of reflections shown in Figure 14 are {110} type spots, which are due to double diffraction.

Figures 8b and 13, and 15b and 16b (discussed below), are dark field micrographs taken using {112} type reflections. In all four of these figures the precipitates can be seen to lie along <112> type directions. Based on the literature the <112> type directions shown in

these figures are probably projections of <110> type directions. After aging the solution-annealed-and-quenched material for 1,525 minutes at 1500^{0}C, light and dark bands could be seen to run throughout the material (Figures 15a). Figure 15b is a dark field view of 15a, showing precipitates brightly lit up in only one direction. These precipitates were found to be 0.03μm wide and 0.40μm long. Further aging, for a total of 10,080 minutes at 1500^{0}C, brought about the formation of long cylindrical particles that ran throughout the grains. Depending on the contrast conditions, the cylindrical particles sometimes appeared to be banded with alternate light and dark regions, as shown in Figure 16a. A dark-field micrograph of an area similar to that shown in Figure 16a is shown in 16b. In this figure it can be seen that only alternate bands, in the banded particles, showed up brightly. Aging the material for 10,080 minutes at 1500^{0}C was found to cause the precipitates to grow to a size of 0.10μm wide and 0.50μm long.

X-ray diffractometer analysis, optical microscopy, and transmission electron microscopy of the material aged for 10,080 minutes showed that a small percentage, approximately 5%, of monoclinic phase was present along the grain boundaries. The developement of this grain boundary phase is probably what causes the microhardness to drop (see Figure 12) after reaching a peak of 1517 kg/mm^2 after 250 minutes at 1500^{0}C. A twinned monoclinic grain boundary precipitate is shown in Figure 17. An optical micrograph of the solution-annealed material after aging for 10,080 minutes is shown in Figure 18. Note that there are many grain boundary precipitates.

The structures of the aged and unaged specimens were also studied by X-ray analysis with a diffractometer using CuKα radiation. X-ray analysis also demonstrated that the amount of strain within the material decreased with aging time at 1500^0C. This reduction in strain is indicated by the fact that the diffraction peaks become narrower and more intense with increasing aging time as shown in Figure 19. The portion of the diffractometer scans shown contains the cubic (400) and the tetragonal (400) and (004) peaks. Because the cubic and tetragonal lattice parameters are only slightly different, these peaks are difficult to separate.

When CaO- or MgO-PSZ (10,11,13) is ground into powder form for X-ray analysis, the metastable tetragonal precipitates retained at room temperature transform to monoclinic because of the removal of the contraint of the matrix. This transformation also occurs in the vicinity of cracks which propagate through the material and is believed to enhance the toughness of the PSZ. This toughening mechanism has been called transformation toughening. However, it has been reported that the tetragonal precipitates in Y_2O_3-PSZ do not transform to monoclinic on grinding (10). Similar results were also obtained in this study. Grinding was found to have little if any influence on the percentage of monoclinic phase. Thus, it appears that transformation toughening is not a significant mechanism in Y_2O_3-PSZ. The improved properties of this material are probably primarily associated with precipitation strengthening instead.

The fracture toughness of the solution-annealed-and-quenched material and of the same material after aging was measured using an overloaded microhardness testing machine. In all cases the fracture toughness was found to be between 2 and 3 $MN/m^{3/2}$. The fracture toughness of our material and those of several other PSZ's are given in a table in Figure 20. From the table, it can be seen the PSZ's that don't transformation toughen, which includes ours, have K_c's (fracture toughnesses) between 1 and 3, while PSZ's that do transformation toughen have K_c's between 5 and 9.

Conclusions

1. The commercially available 8.0 weight-percent Y_2O_3-PSZ studied contains a few large spheroidal and grain boundary precipitates up to 4μm in size which are either metastable tetragonal or monoclinic in structure and small 0.06μm tetragonal precipitates arranged in a tweed pattern.
2. Spheroidal precipitates up to 1.26μm in diameter were metastable tetragonal; large spheroidal precipitates transformed to monoclinic.
3. Solution annealing and quenching the PSZ dissolved all of the precipitates but very fine 0.02μm tetragonal particles formed in a tweed configuration during the air quench.
4. The as-received PSZ exhibited a typical hardening behavior showing a maximum hardness of about 1400 kg/mm^2 after 50 minutes at 1500^{0}C.
5. During aging at 1500^{0}C the fine tetragonal precipitates in the as-received PSZ grew from 0.06 to 0.12μm in 250 minutes.
6. The solution-annealed-and-quenched PSZ exhibited a much more sluggish hardening behavior than the as-received PSZ and it reached a maximum hardness of 1517 kg/mm^2 after 250 minutes at 1500^{0}C.
7. Aging the solution-annealed-and-quenched PSZ caused the 0.02μm tetragonal precipitates, which were almost spherical, to grow and form a structure that is made up of elongated banded particles. These particles are made up of the tetragonal precipitates which are, after aging for 10,080 minutes at 1500^{0}C, approximately 0.10μm wide and 0.50μm long.

8. The drop in hardness observed upon aging the solution-annealed-and-quenched material for long times is associated with the formation of grain boundary monoclinic precipitates.
9. Grinding the Y_2O_3-PSZ into a powder did not cause a significant amount of metastable tetragonal to transform to monoclinic. This fact implies that transformation toughening is not a significant mechanism in Y_2O_3-PSZ.
10. The fracture toughness of the solution-annealed-and-quenched material, aged and unaged, was found to be between 2 and 3 $MN/m^{3/2}$. These values are similar to those of other PSZ's that do not exhibit transformation toughening.

References

1. E. R. Thompson, "Directional Structures for Advanced Aircraft Turbine Blades", Journal of Aircraft, May 1977.

2. C. H. Liebert and F. S. Stepka, "Potential Use of Ceramic Coating as a Thermal Insulation on Cooled Turbine Hardware", NASA TM X-3352, 1976.

3. C. H. Liebert, R. E. Jacobs, S. Stecura, and R. C. Morse, "Durability of Zirconia Thermal Barrier Ceramic Coatings on Air-Cooled Turbine Blades in Cyclic Jet Engine Operation", NASA TM X-3410.

4. S. Stecura and C. H. Liebert, "Thermal Barrier Coating System", U.S. Patent no. 4,055,705. Oct. 1977.

5. S. Stecura, "Two-Layer Thermal Barrier Coating for Turbine Airfoils-Furnace and Burner Rig Test Results", NASA TM X-3425, 1976.

6. S. Stecura, "Two-Layer Thermal Barrier Coating for High Temperature Components", American Ceramics Society Bulletin, Vol. 56, 1977, pp. 1082-1085.

7. S. Stecura, "Effects of Compositional Changes on the Performance of a Thermal Barrier Coating System", NASA TM 78976.

8. A. G. Evans and E. A. Charles, "Fracture Toughness Determination by Indentation", Journal of the American Ceramic Society, Vol. 59, 1976, pp. 371-372.

9. Kato, Masaharu, Monzen, Ryoichi, and Mori, T. (1978), Acta Met., Vol. 26, 605-613.

10. Hannink, R. H. J. (1978), J. of Mat. Sci., 13, 2487-2496.

11. Garvie, R. C., Hannink, R. H., and Pascoe, R. T. (December 25, 1975), Nature, Vol. 258, 703-704.

12. Gupta, T. K., Bechtold, J. H., Kuznicki, R. C., Cadoff, L. H., and Rossing, B. R. (1977), J. of Mat. Sci., 12, 2421-2426.

13. Porter, D. L. (1977), Ph.D. Thesis; Case Western Reserve Univ., Cleveland, Ohio 44106.

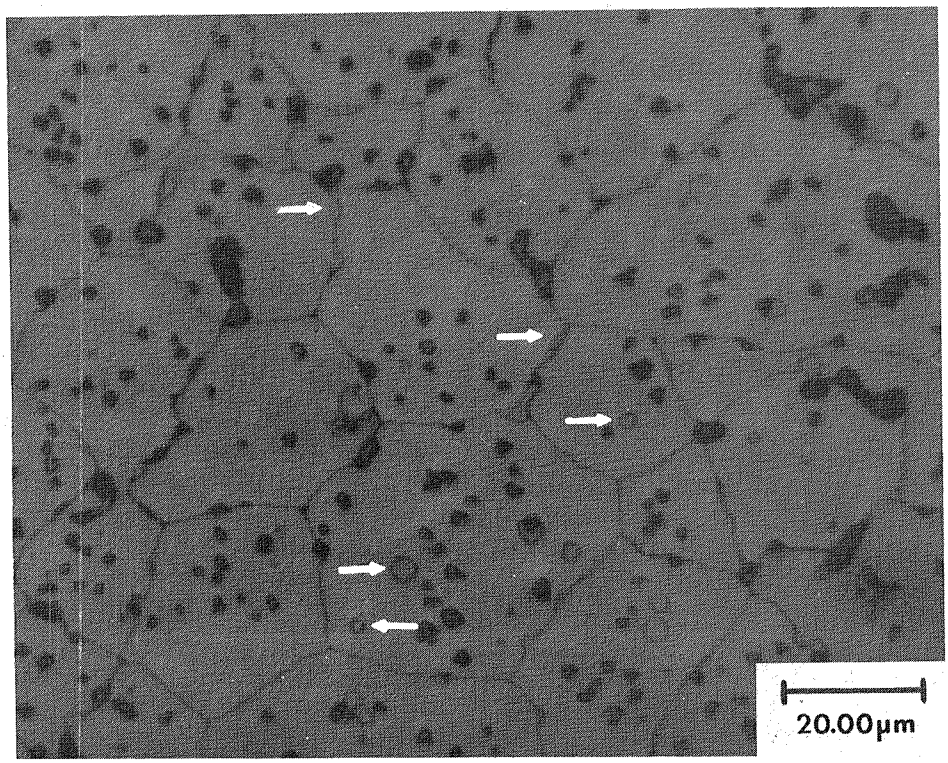

Figure 1:

Light micrograph showing the commercially produced 8 wt.-% Y_2O_3–PSZ in the as-received condition. Note the many grain boundary precipitates and spheroidal particles, some of which are arrowed (915X).

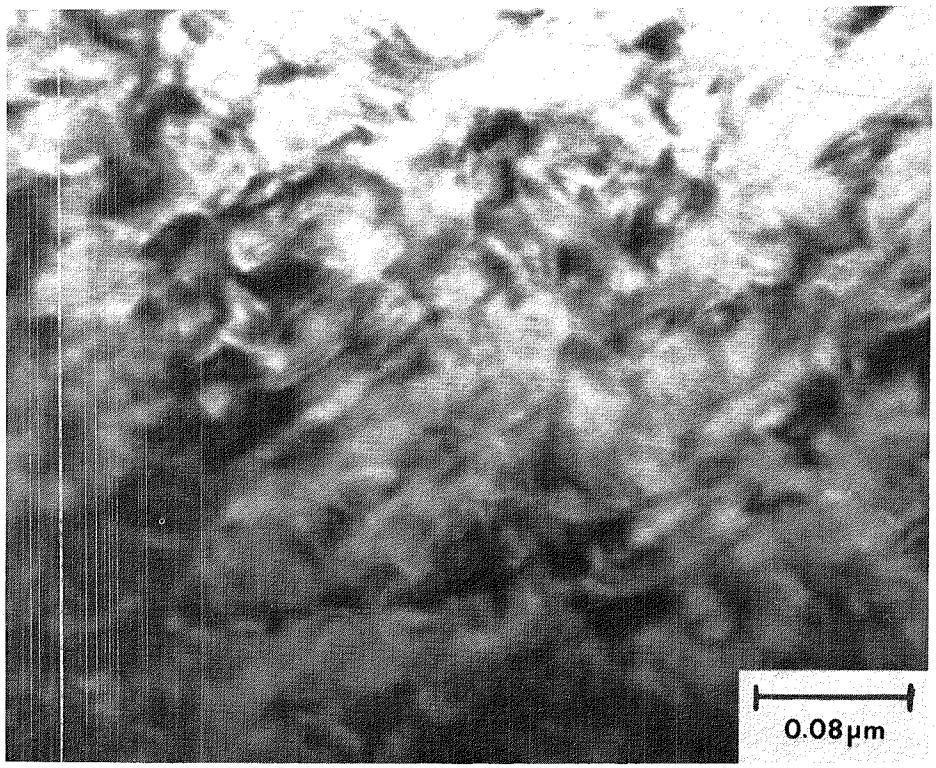

Figure 2:

(A) Bright-field transmission electron micrograph (100kv) of the as-received 8 wt.-% Y_2O_3-PSZ. This micrograph shows strain contrast (252,000X).

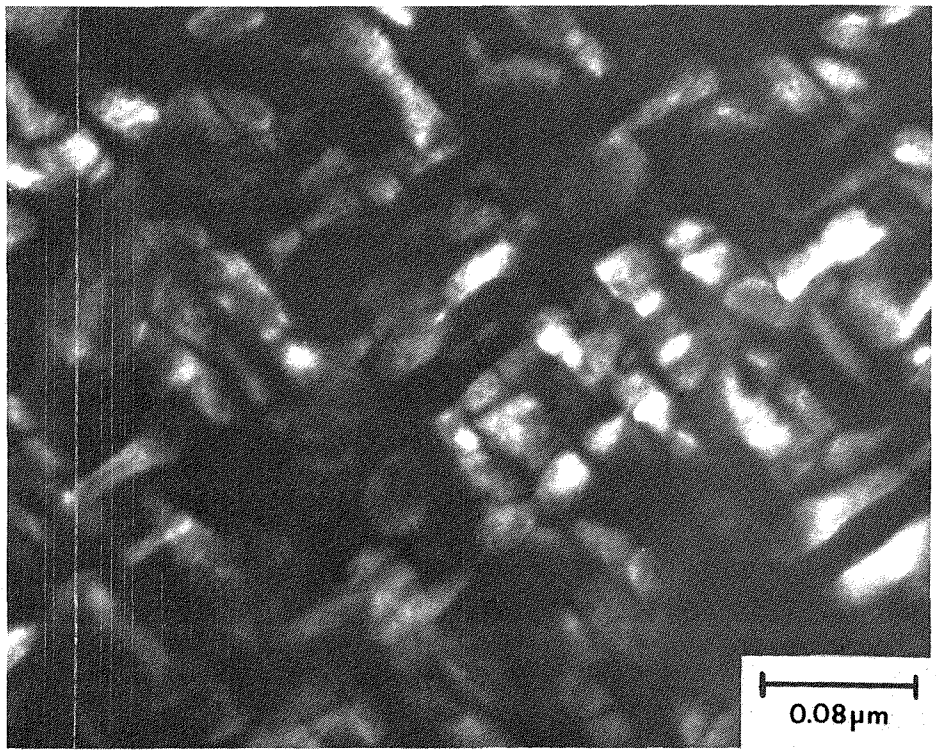

Figure 2:

(B) Dark-field transmission electron micrograph (100kv) of the same area shown in (A) showing coherent tetragonal precipitates (0.06 μm) in a cubic matrix (252,000X).

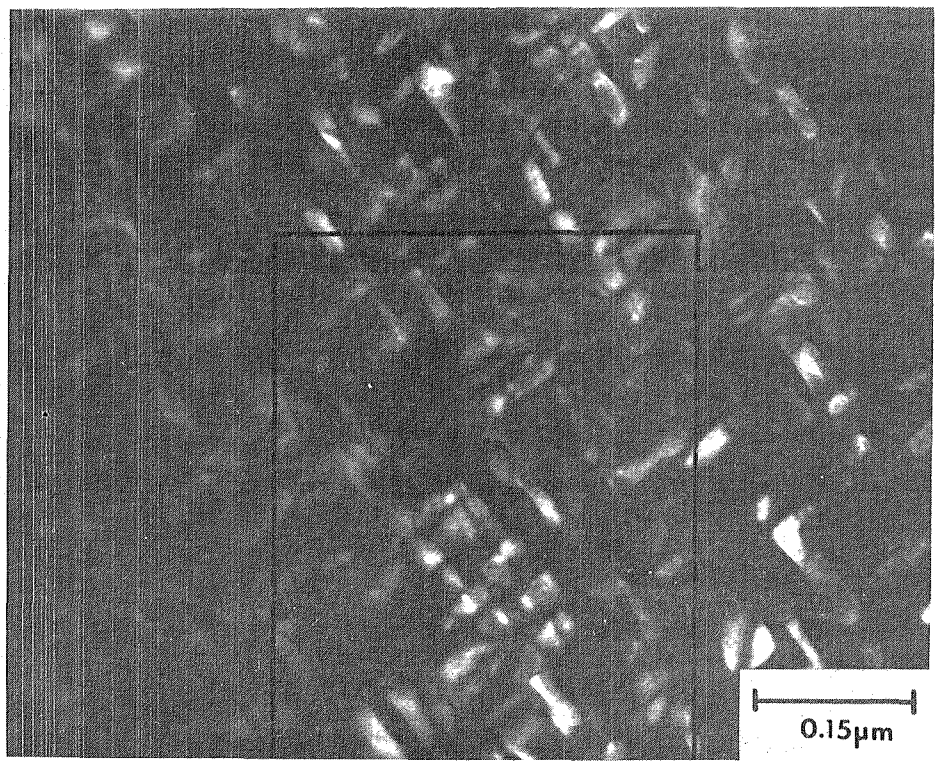

Figure 2:

(C) Dark-field transmission electron micrograph (100kv) of an area that includes the area shown in (A) and (B) (the rectangular area in the center of the micrograph) showing coherent tetragonal precipitates in a cubic matrix (142,200X).

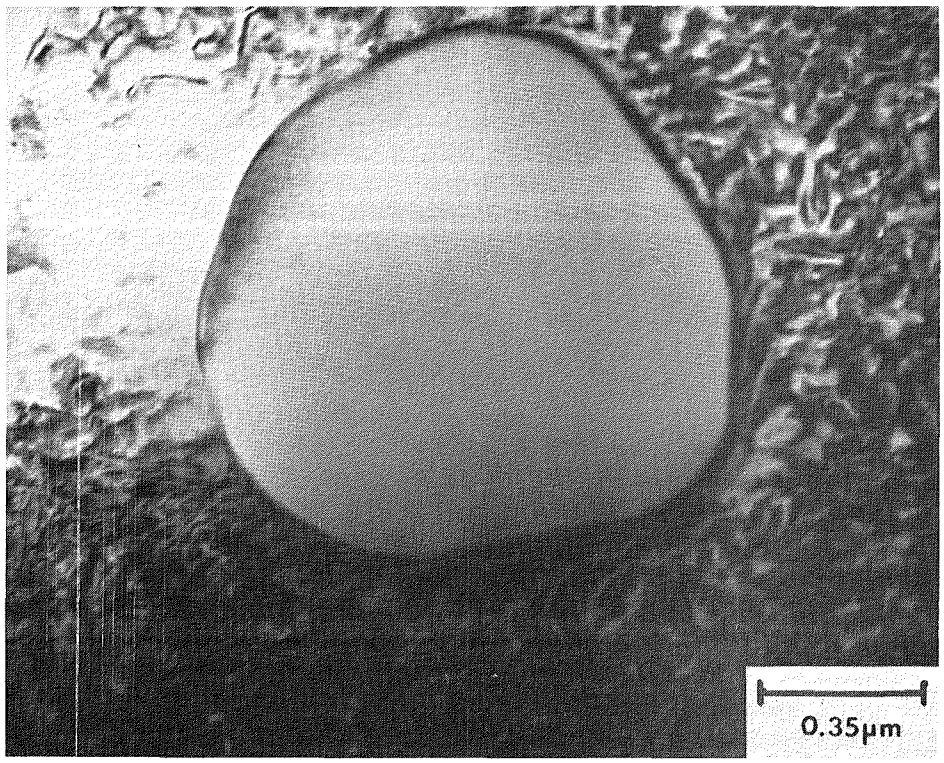

Figure 3:

Bright-field transmission electron micrograph (125kv) of the as-received 8 wt.-% Y_2O_3-PSZ. This micrograph shows a 1.26µm spheroidal precipitate. Strain contrast is evident in the grain surrounding the precipitate (59,100X).

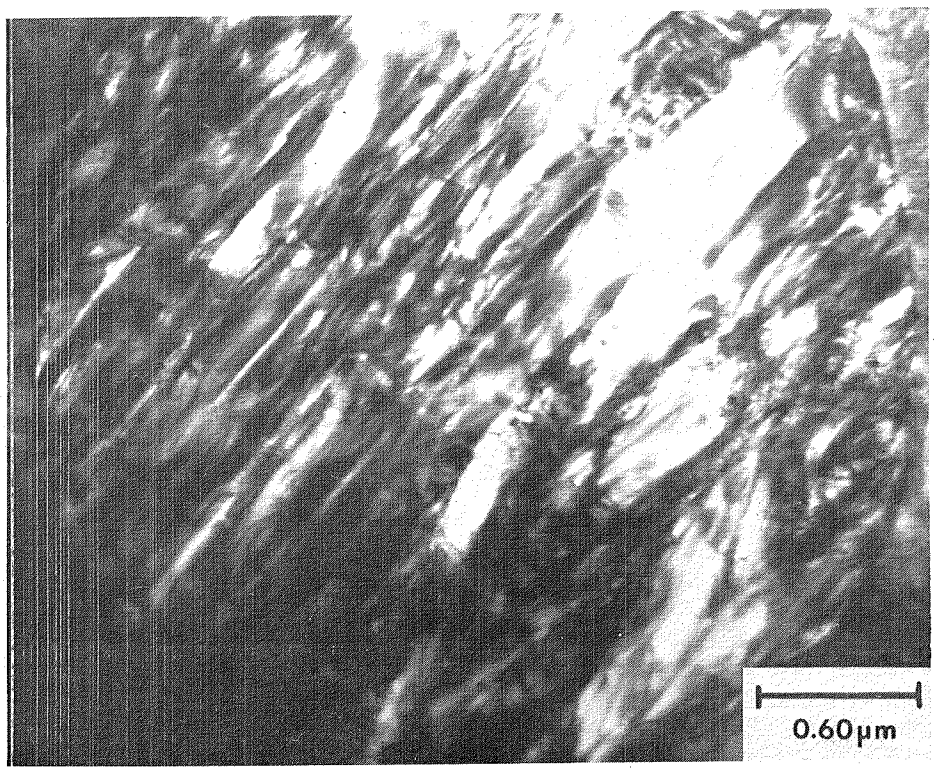

Figure 4:

(A) Bright-field transmission electron micrograph (125kv) of the as-received 8 wt.-% Y_2O_3-PSZ, showing a twinned 3.50µm spheroidal monoclinic precipitate (35,100X).

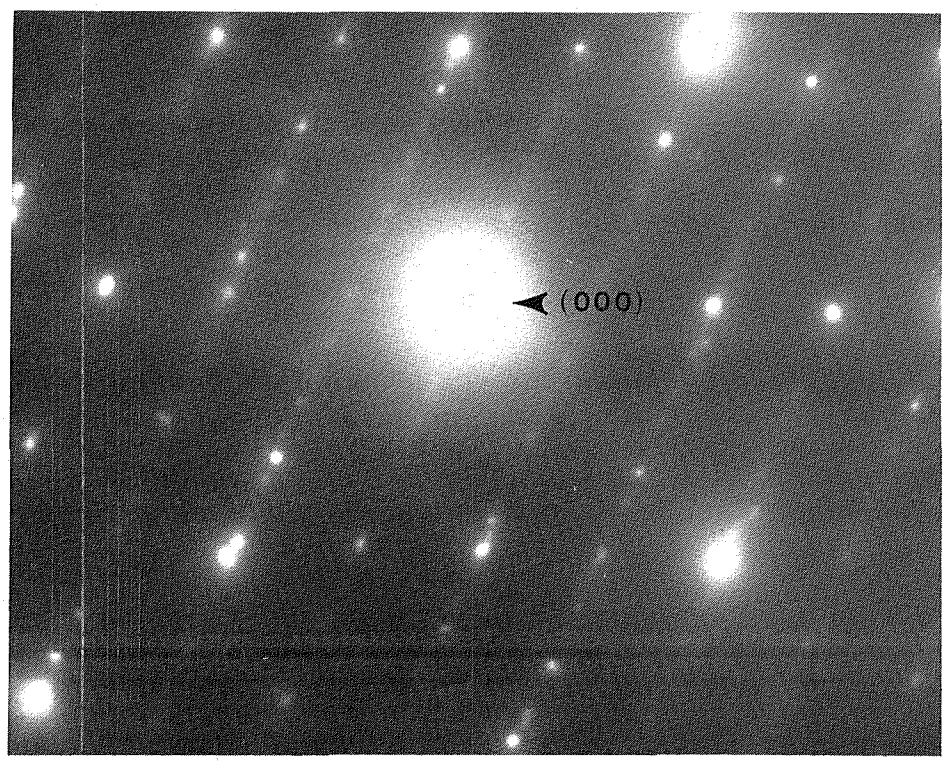

Figure 4:

(B) Selected-area-diffraction pattern (125kv) of the precipitate shown in (A) showing the transmitted spot (000) used to form image (A).

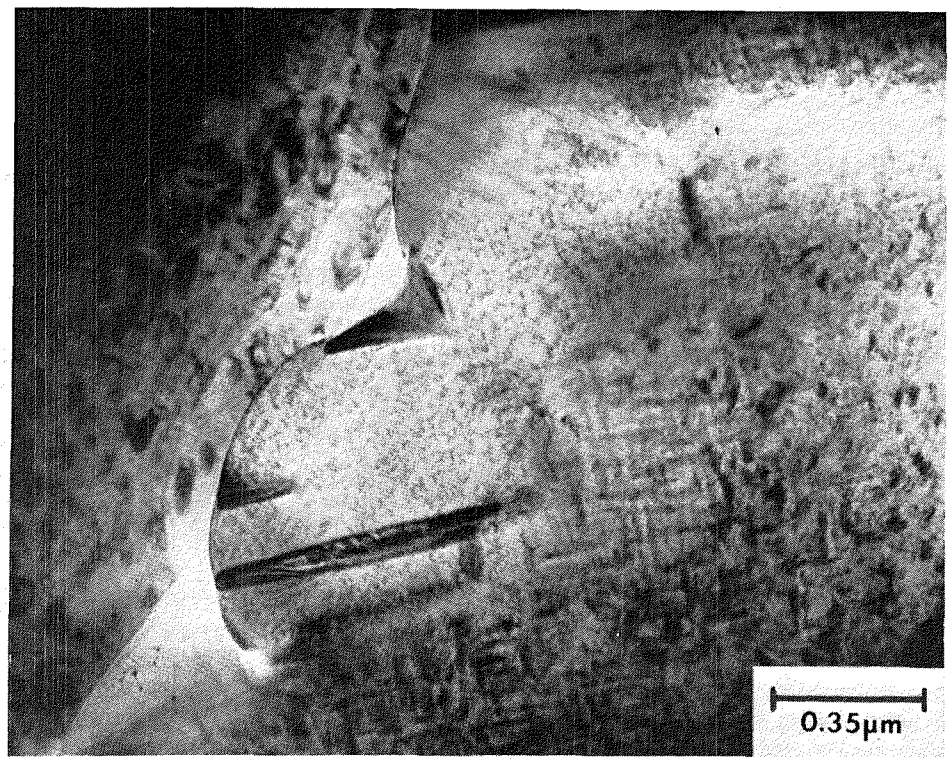

Figure 5:

Bright-field transmission electron micrograph (125kv) of the as-received 8 wt.-% Y_2O_3-PSZ, showing a grain boundary precipitate. Strain contrast is evident in the grains adjacent to the precipitate (59,100X).

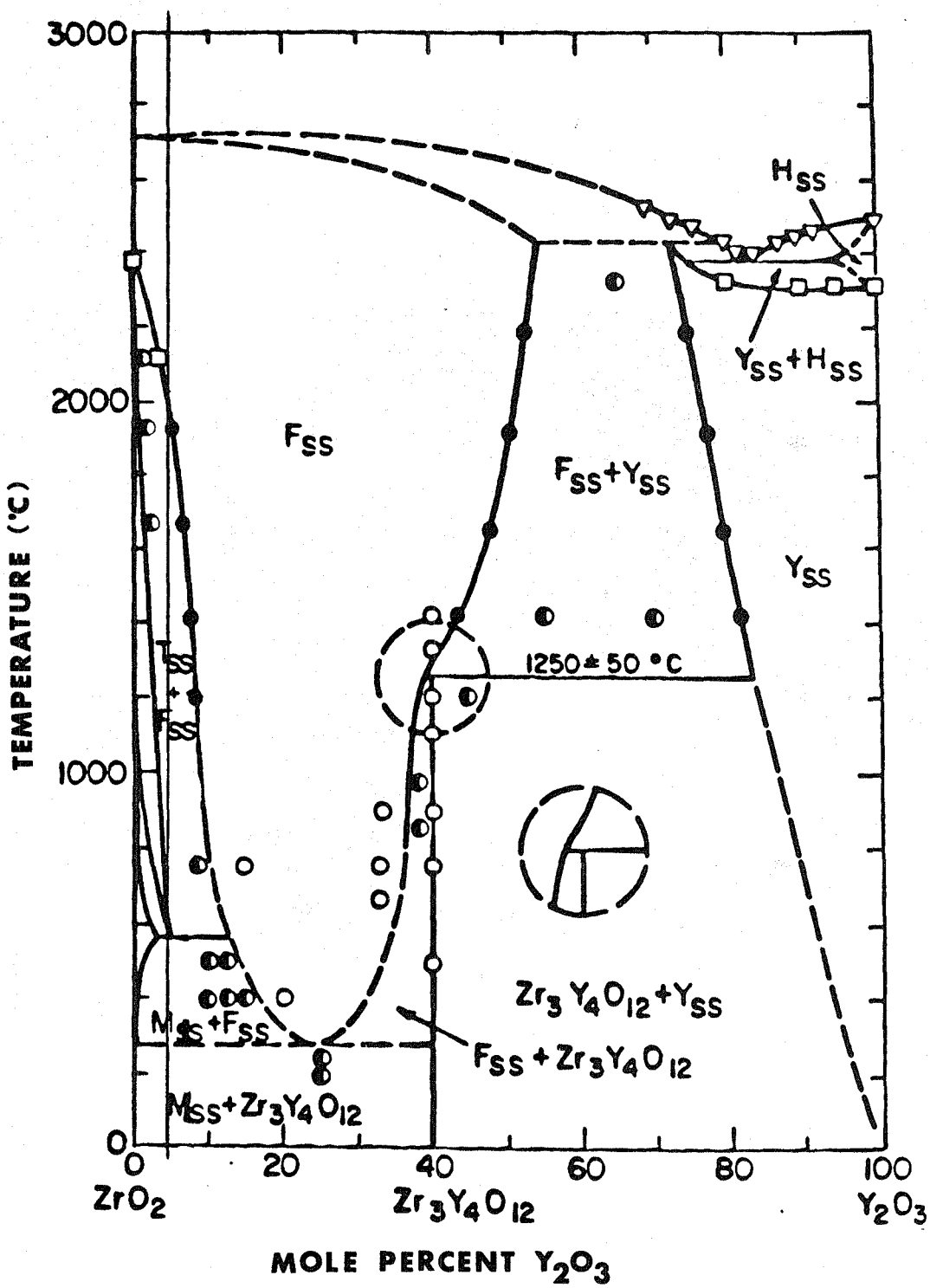

Figure 6:

Equilibrium phase diagram for the system ZrO_2-Y_2O_3 (Stubican, V. S., Hink, R. C., and Ray, S. P. (1978), J. Am. Ceram. Soc. 61, 17.).

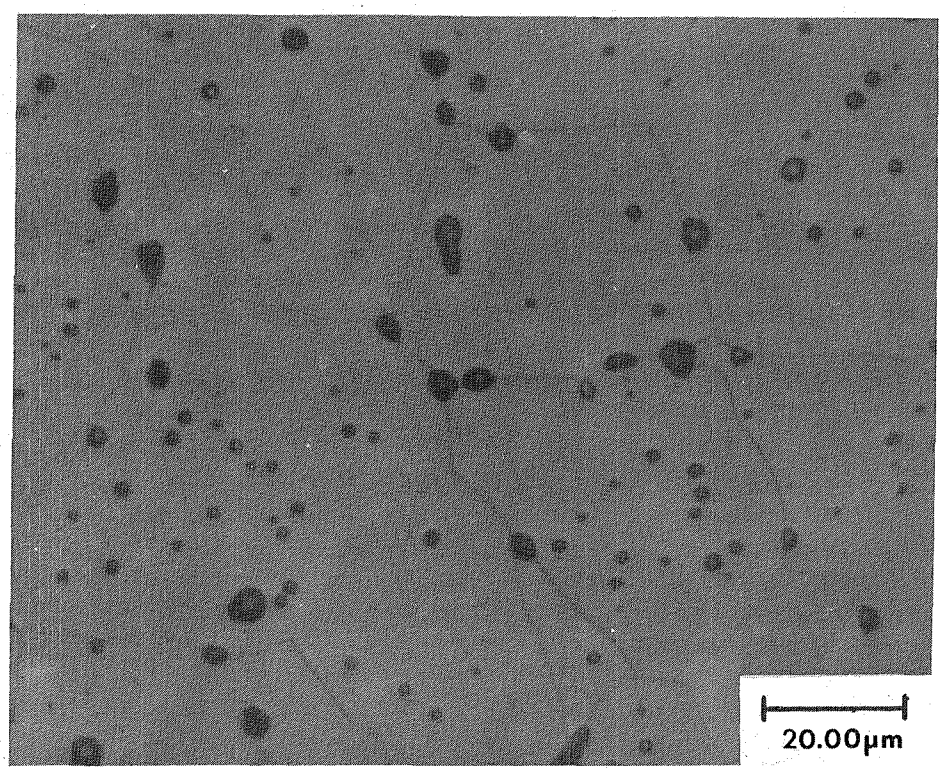

Figure 7:

Light micrograph showing the solution-annealed-and-quenched 8 wt.-% Y_2O_3-PSZ. Note the absence of grain boundary precipitates and spheroidal particles (915X).

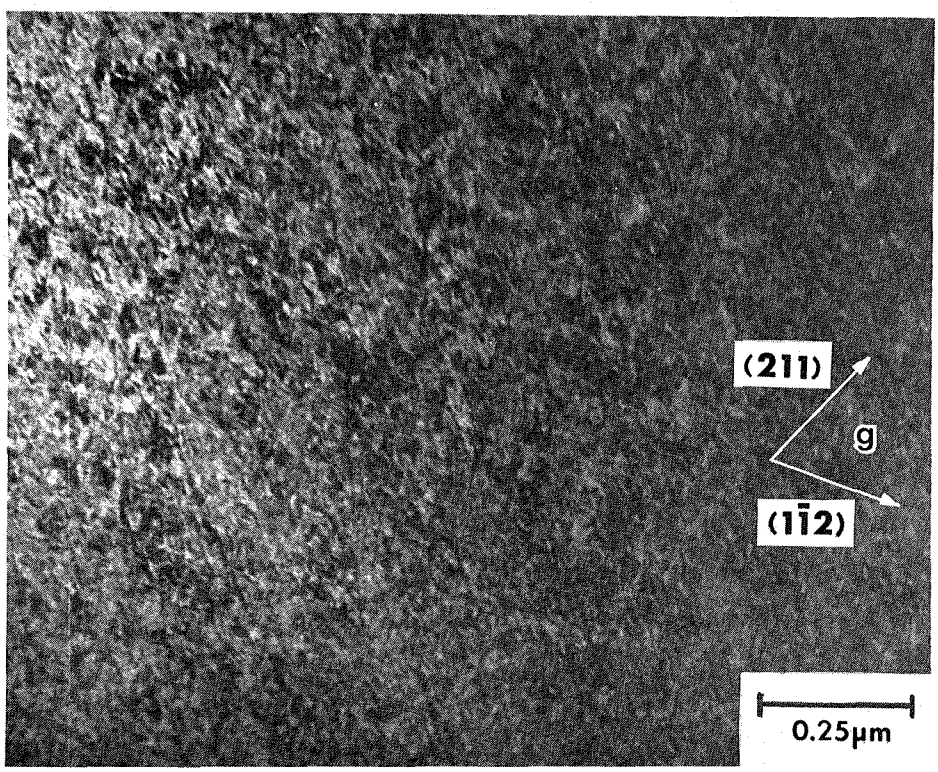

Figure 8:

(A) Bright-field transmission electron micrograph (125kv) of the solution-annealed-and-quenched 8 wt.-% Y_2O_3-PSZ. This micrograph shows strain contrast (80,200X).

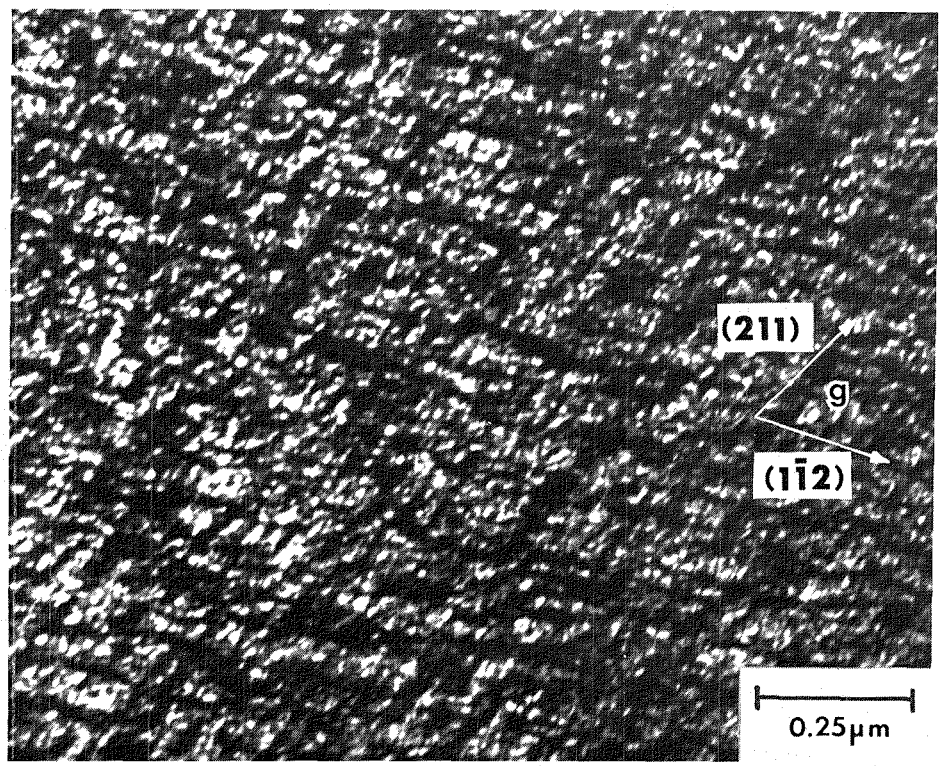

Figure 8:

(B) Dark-field transmission electron micrograph (125kv) of the same area shown in (A) showing coherent tetragonal precipitates (0.02 μm) in a cubic matrix. Note that the particles lie in two <112> type directions (80,200X).

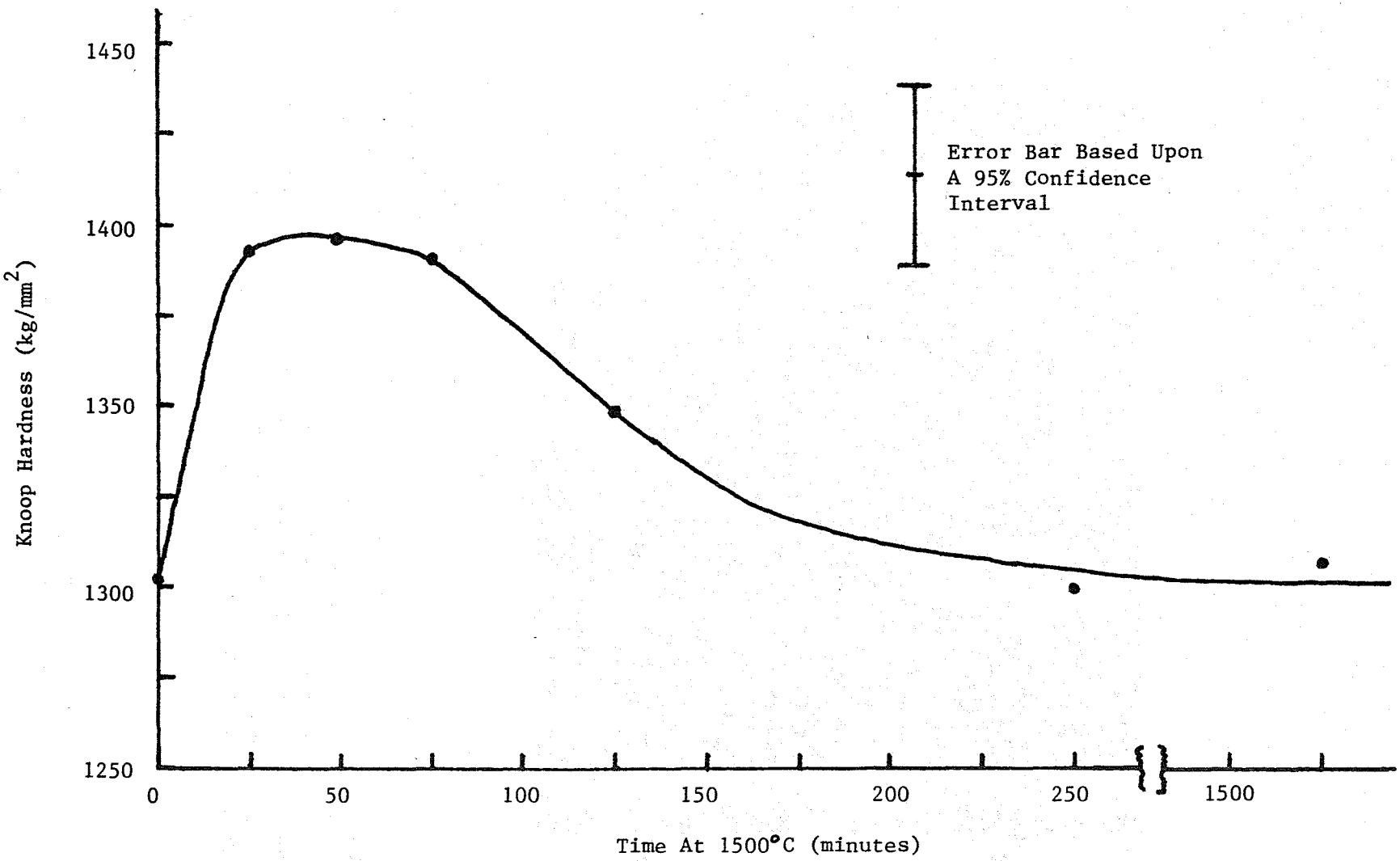

Figure 9: Microhardness of a commercially available bulk 8.0 wt.-% Y_2O_3-PSZ as a function of aging time at 1500°C. Microhardness was measured using a knoop diamond indenter and 200gm load.

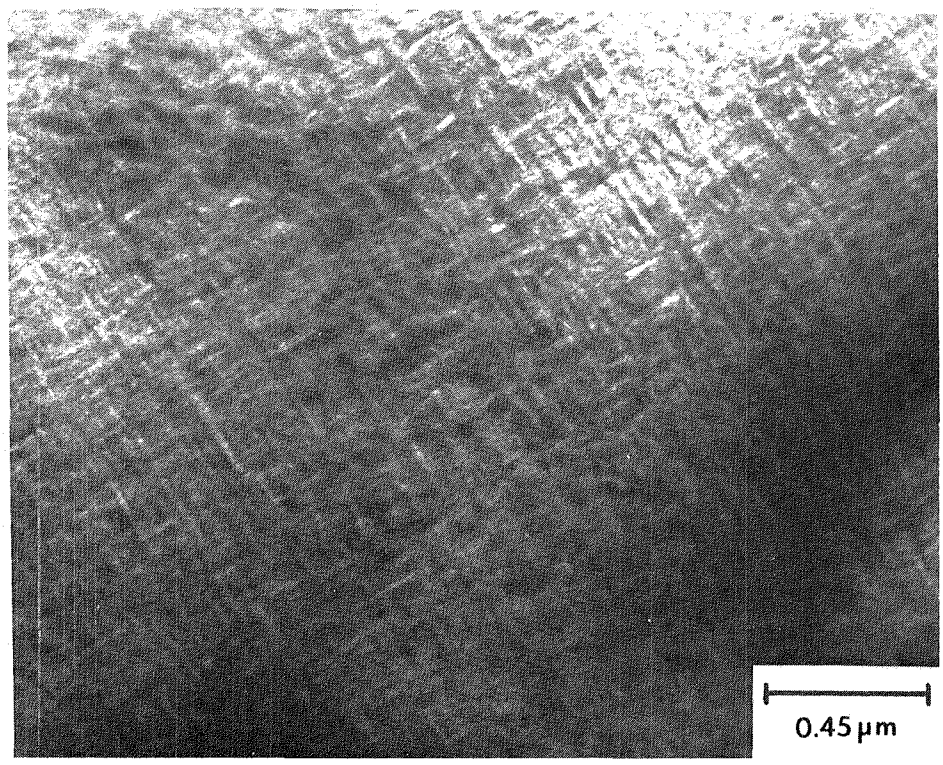

Figure 10:

Dark-field transmission electron micrograph (125kv) of the as-received 8 wt.-% Y_2O_3-PSZ that was held at 1500°C for 50 minutes and then quenched. This micrograph shows a cross-hatch pattern (47,000X).

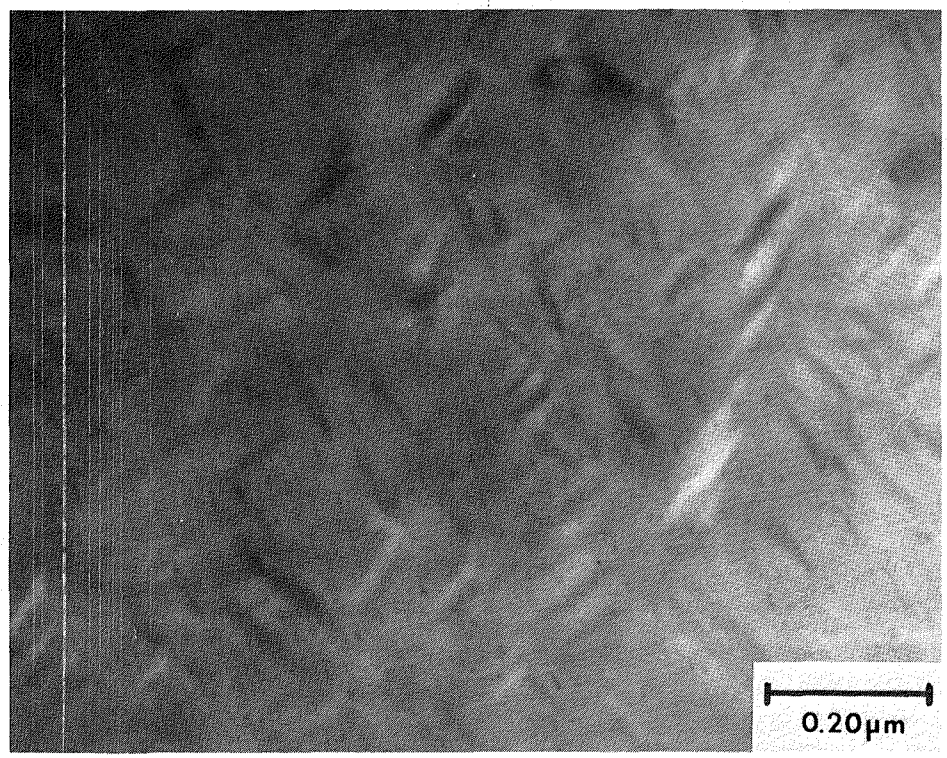

Figure 11:

(A) Bright-field transmission electron micrograph (125kv) of the as-received 8 wt.-% Y_2O_3-PSZ that was held at 1500°C for 250 minutes and then quenched. This micrograph shows coherent tetragonal precipitates (0.12μm) in a cubic matrix (108,900X).

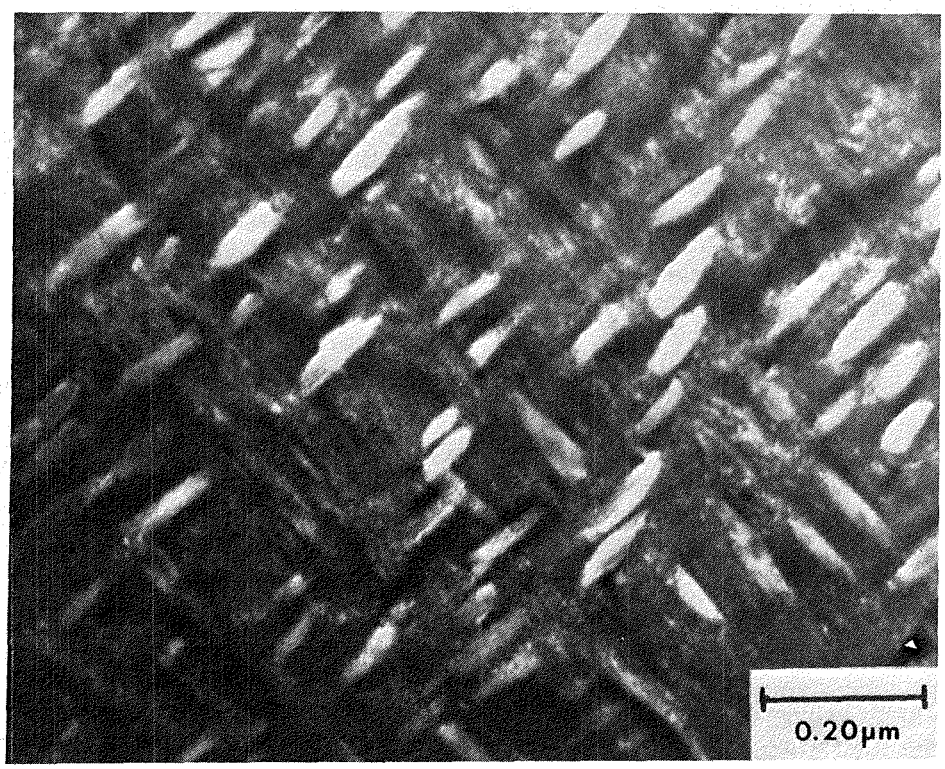

Figure 11:

(B) Dark-field transmission electron micrograph (125kv) of the same area shown in (A) showing coherent tetragonal precipitates in a cubic matrix (108,900X).

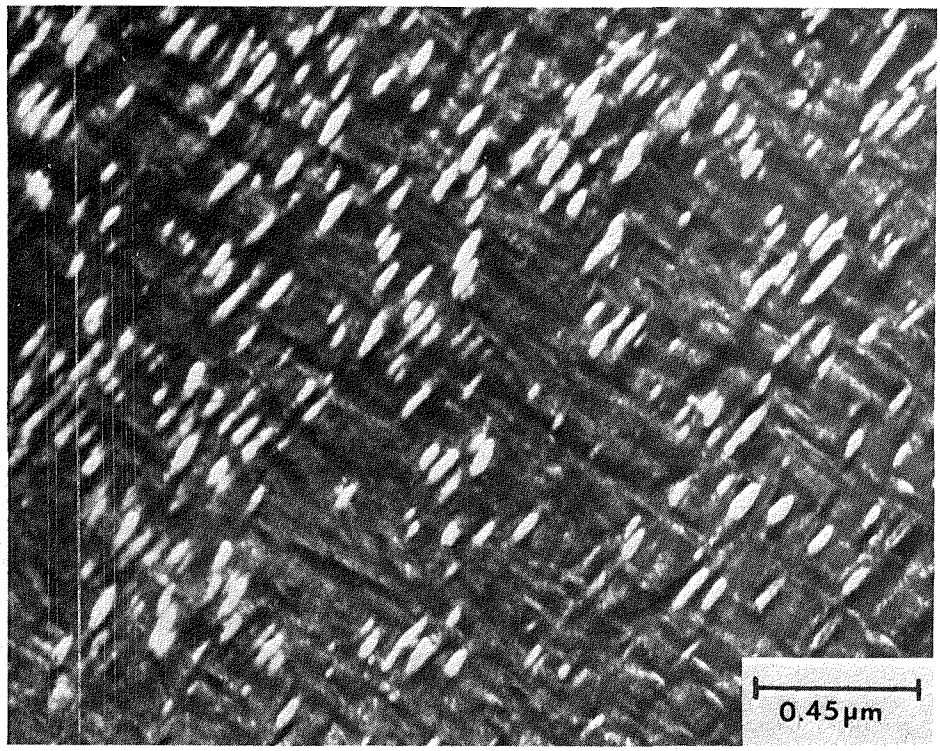

Figure 11:

(C) Dark-field transmission electron micrograph (125kv) of an area from the same grain that was used for (A) and (B) showing coherent tetragonal precipitates in a cubic matrix (47,000X).

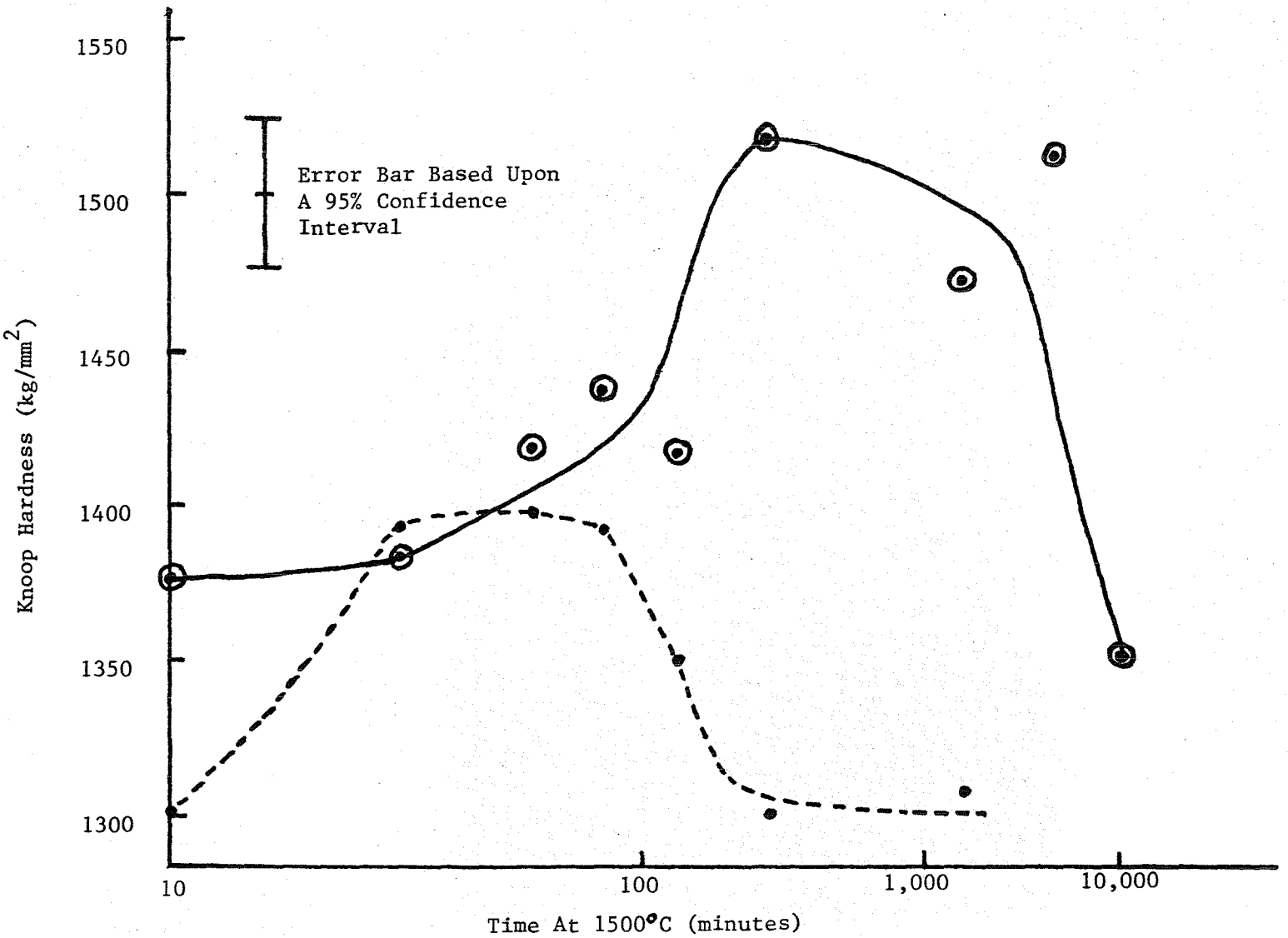

Figure 12: Microhardness of the solution-annealed-and-quenched 8.0 wt.-% Y_2O_3-PSZ as a function of aging time at 1500°C. For the sake of comparison the microhardness curve for the commercially available (as-received) bulk material is shown above as a dashed line (also see Figure 9). Microhardness was measured using a knoop diamond indenter and 200gm load.

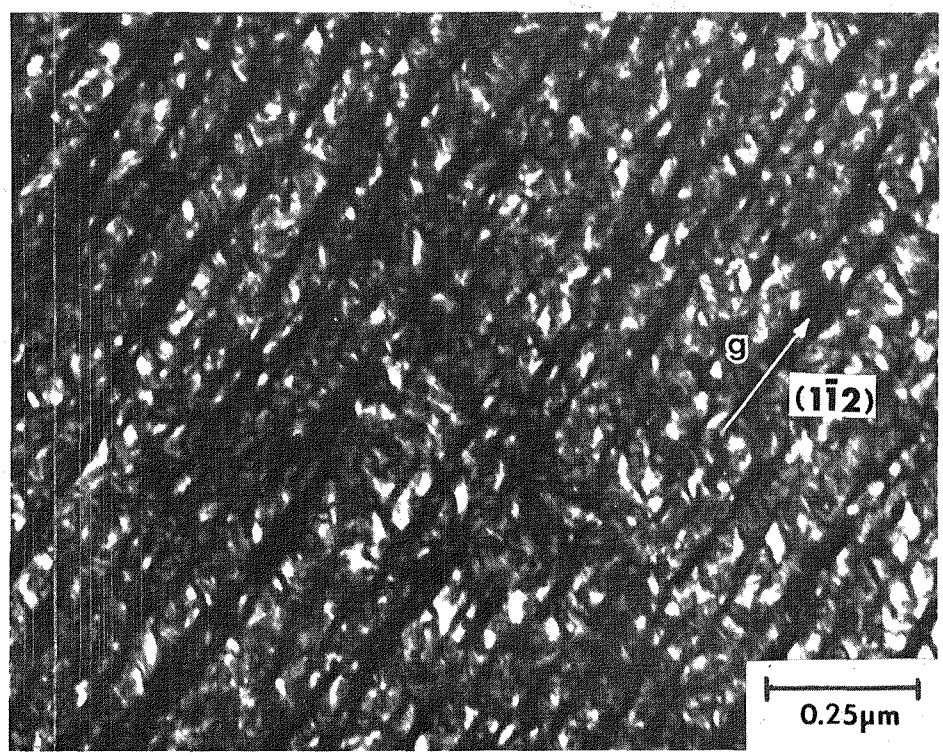

Figure 13:

Dark-field transmission electron micrograph (125kv) of the solution-annealed-and-quenched 8 wt.-% Y_2O_3-PSZ that was held at 1500° C for 50 minutes and then quenched. This micrograph shows coherent tetragonal precipitates (0.04μm) that are aligned in a <112> type direction (80,200X).

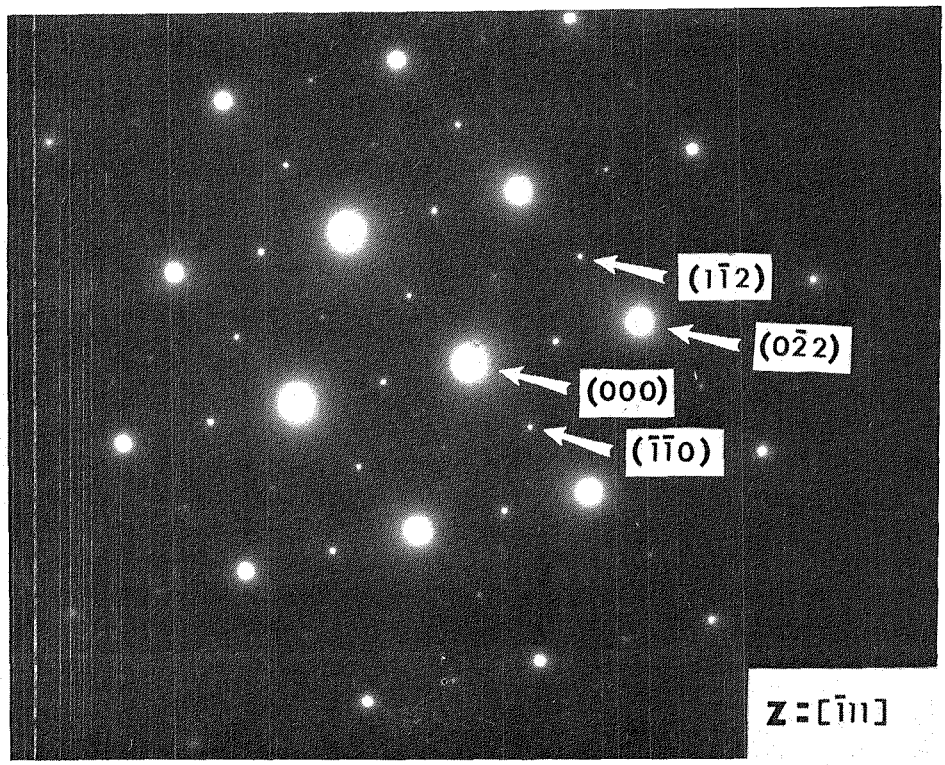

Figure 14:

Selected-area-diffraction pattern (125kv) that is typical of those obtained from the areas shown in the micrographs of the aged and unaged solution-annealed-and-quenched specimens. The SAD pattern is that of a [$\bar{1}$1$\bar{1}$] zone. Besides the transmitted spot, (000), three types of spots are pointed out by arrows; they are as follows: cubic matrix spots of {220} type (ex. (0$\bar{2}$2)), superlattice tetragonal spots of {112} type (ex. (1$\bar{1}$2)), and double diffraction spots of {110} type (ex. ($\bar{1}\bar{1}$0)).

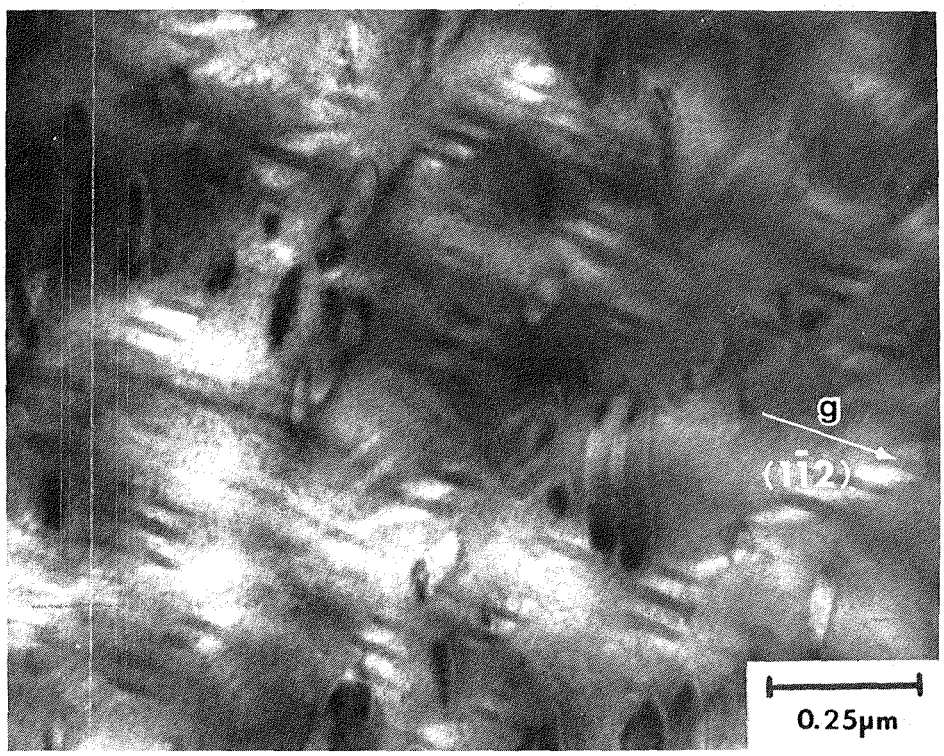

Figure 15:

(A) Bright-field transmission electron micrograph (125kv) of the solution-annealed-and-quenched 8 wt.-% Y_2O_3-PSZ that was held at 1500 °C for 1525 minutes and then quenched. This micrograph shows banded particles whose "bands" all lie in the same direction, a <112> type (80,200X).

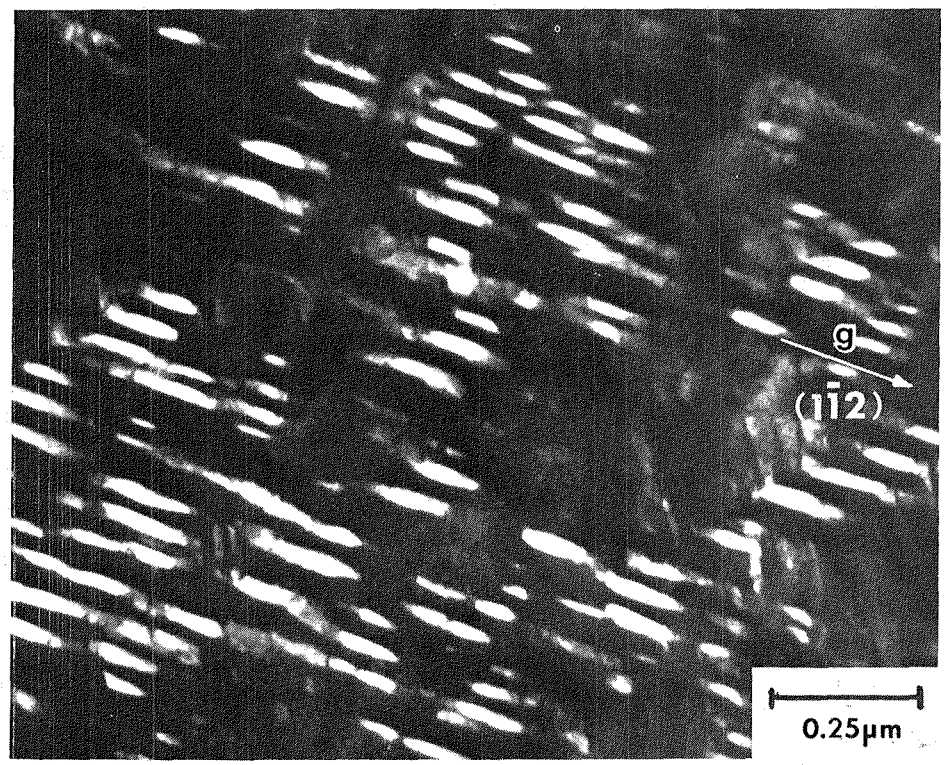

Figure 15:

(B) Dark-field transmission electron micrograph (125kv) of the same area shown in (A) showing coherent tetragonal precipitates in a cubic matrix. The precipitates (0.03μm wide and 0.40μm long) are aligned in a <112> type direction (80,200X).

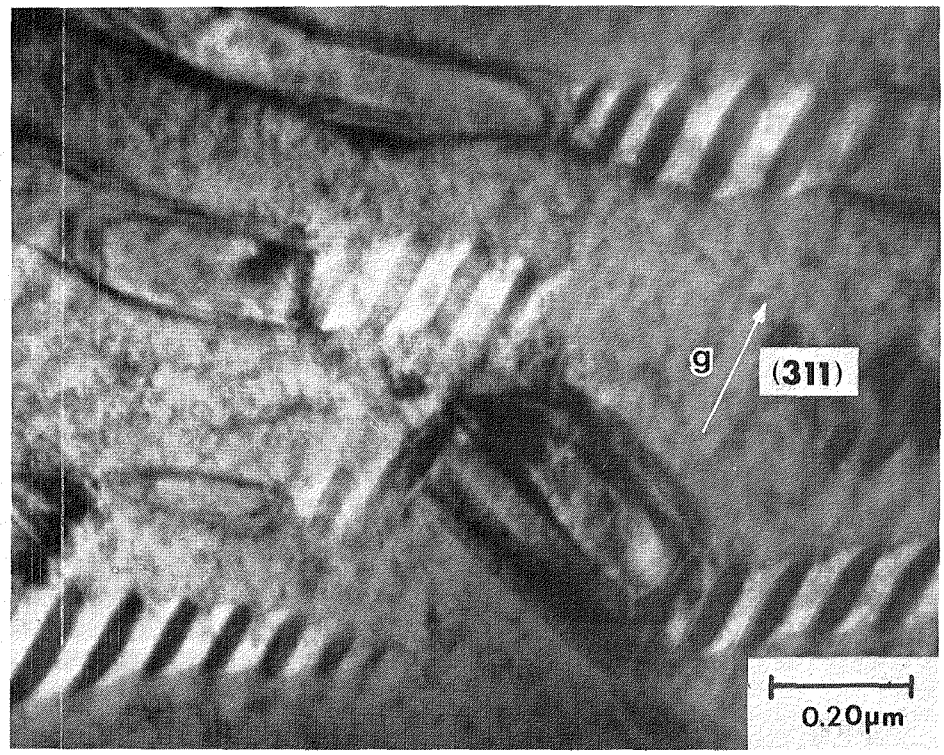

Figure 16:

(A) Bright-field transmission electron micrograph (125kv) of the solution-annealed-and-quenched 8 wt.-% Y_2O_3-PSZ that was held at 1500 °C for 10,080 minutes and then quenched. This micrograph shows that the structure is now comprised mainly of long particles of tetragonal phase running through a cubic matrix. Note the bands in some of the particles that are due to differences in the contrast of the different variants. The "bands" in this micrograph lie along a <113> type direction (97,600X).

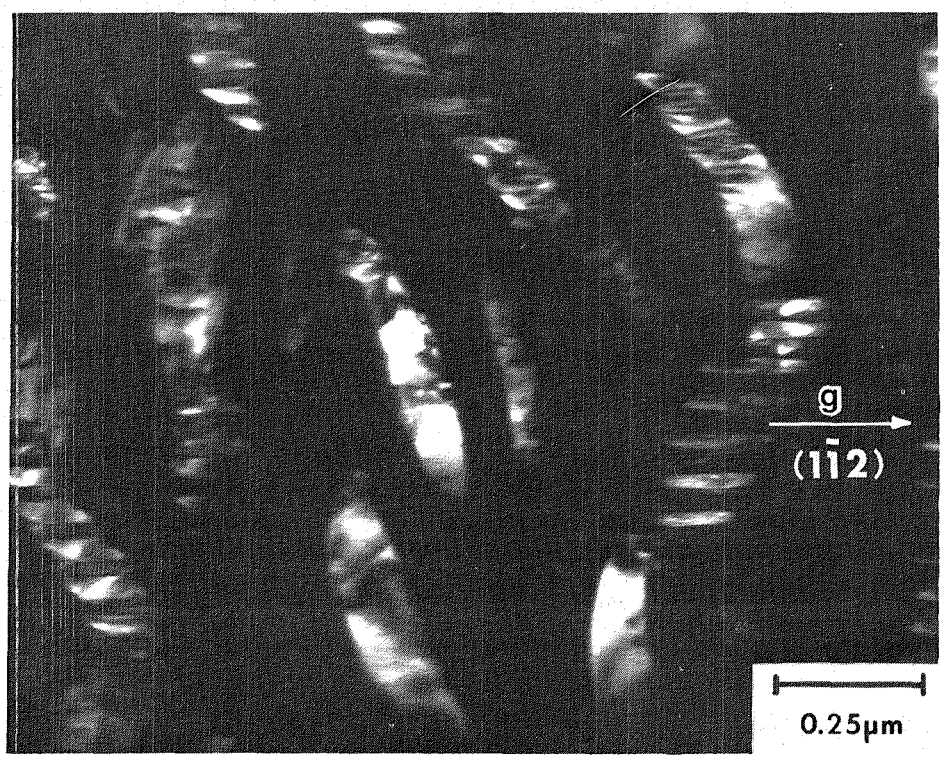

Figure 16:

(B) Dark-field transmission electron micrograph (125kv) of an area similar to that shown in (A) showing coherent tetragonal precipitates in a cubic matrix. The precipitates (0.10μm wide and 0.50μm long) are aligned in a <112> type direction (80,200X).

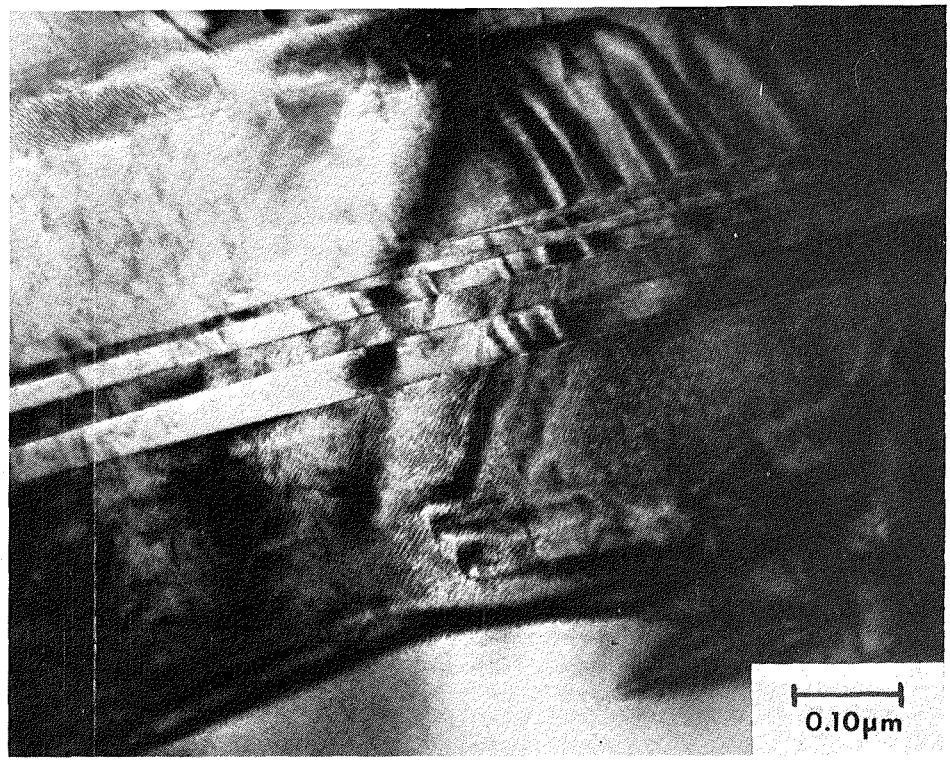

Figure 17:

Bright-field transmission electron micrograph (125kv) of the solution-annealed-and-quenched 8 wt.-% Y_2O_3-PSZ that was held at 1500°C for 10,080 minutes and then quenched. This micrograph shows a twinned monoclinic grain boundary precipitate (127,400X).

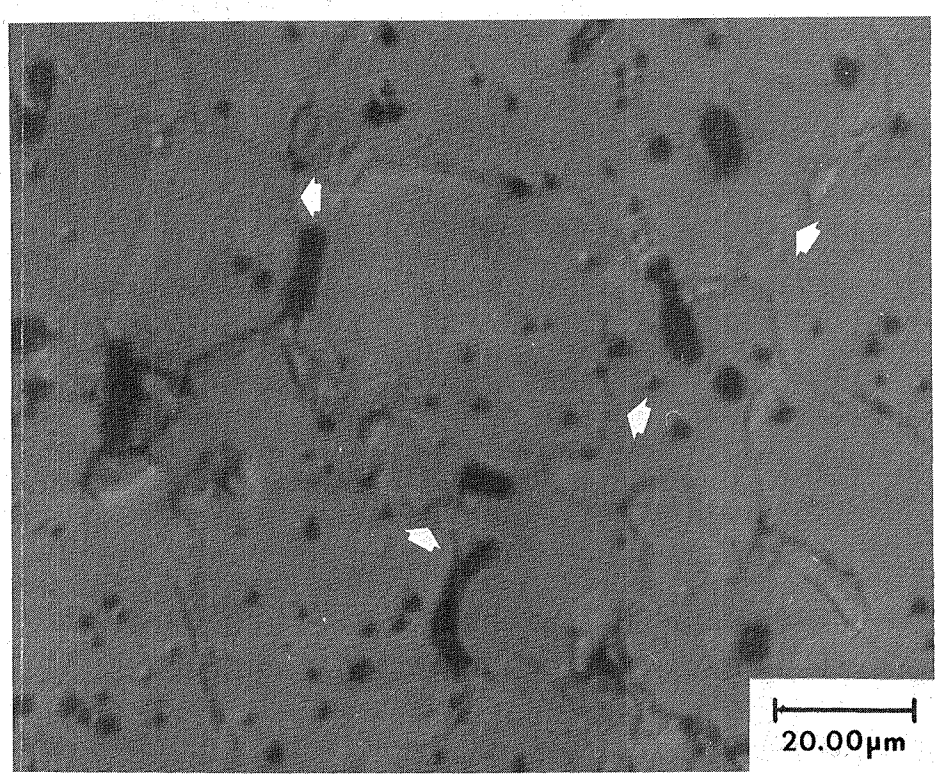

Figure 18:

Light micrograph showing the solution-annealed-and-quenched 8 wt.-% Y_2O_3-PSZ that was held at 1500°C for 10,080 minutes and then quenched. Note the many grain boundary precipitates, some of which are arrowed (915X).

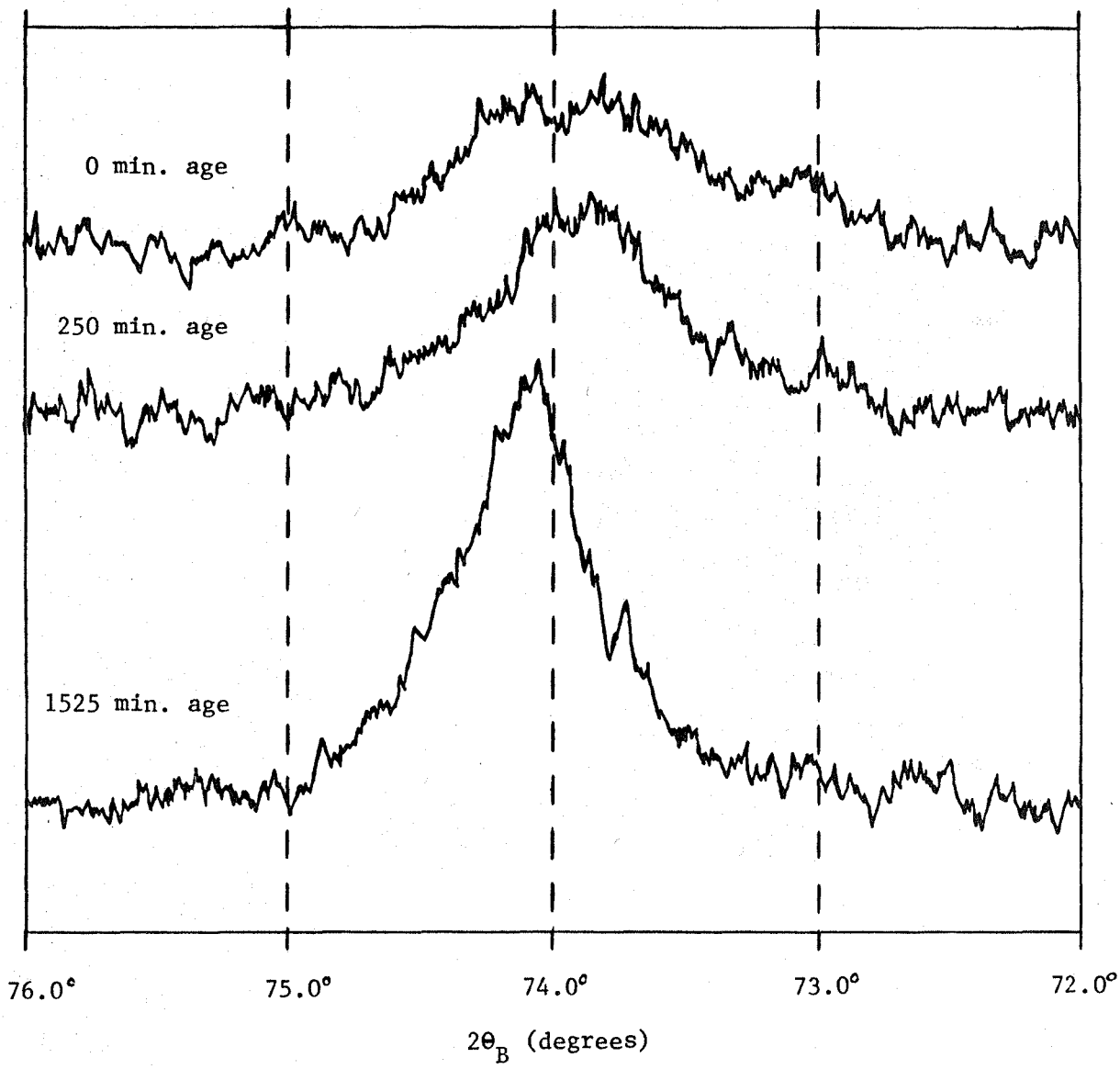

Figure 19:

Influence of aging the as-received material at 1500°C on diffractometer peak configuration. Note the sharpening of the peaks with increasing aging time.

FRACTURE TOUGHNESS OF PSZ

MATERIAL	K_c($MNm^{-3/2}$)	TRANSFORMATION TOUGHENING	REFERENCE
3.4wt%CaO-ZrO_2	1.1	NO	GREEN et. al.
8.1mol%MgO-ZrO_2	5.7	YES	PORTER et. al.
8.1mol%MgO-ZrO_2	2	NO	PORTER et. al.
? wt%Y_2O_3-ZrO_2	6-9	YES	GUPTA et. al.
8.0wt%Y_2O_3-ZrO_2	2-3	NO	PRESENT STUDY

Figure 20:

The fracture toughnesses of several partially stabilized zirconias. Note that PSZ's that don't transformation toughen have K_c's between 1 and 3, while PSZ's that do transformation toughen have K_c's between 5 and 9.

1. Report No.	2. Government Accession No.	3. Recipient's Catalog No.
NASA CR-165126		

4. Title and Subtitle	5. Report Date
MICROSTRUCTURE AND MECHANICAL PROPERTIES OF BULK AND PLASMA-SPRAYED Y_2O_3-PARTIALLY STABILIZED ZIRCONIA	August 1980
	6. Performing Organization Code

7. Author(s)	8. Performing Organization Report No.
Peter G. Valentine and Ralph D. Maier	None
	10. Work Unit No.

9. Performing Organization Name and Address	11. Contract or Grant No.
Case Western Reserve University Cleveland, Ohio 44106	NSG-3252
	13. Type of Report and Period Covered
12. Sponsoring Agency Name and Address	Contractor Report
National Aeronautics and Space Administration Washington, D.C., 20546	14. Sponsoring Agency Code

15. Supplementary Notes

Annual report. Project Manager, Michael A. Gedwill, Jr., Materials Division. NASA Lewis Research Center, Cleveland, Ohio 44135.

16. Abstract

Bulk 8.0 weight-percent yttria partially stabiled zirconia (PSZ) was studied by light microscopy, transmission electron microscopy, X-ray analysis, microhardness testing, and fracture toughness testing. The as-received PSZ contained spheroidal and grain boundary precipitates up to 4 μm in size. Spheroids up to 1.26 μm were metastable tetragonal; large spheroids were monoclinic. Grinding the PSZ into powder did not cause a significant amount of tetragonal to transform to monoclinic. This indicates that transformation toughness is not a significant mechanism in PSZ. Aging the PSZ at 1500^{o} C caused the fine tetragonal precipitates to grow from 0.06 to 0.12 μm, in 250 minutes. A peak hardness of 1400 kg/mm^2 was attained after 50 minutes. Solution annealing and quenching the as-received PSZ eliminated the large precipitates, but fine tetragonal precipitates reformed on quenching. Aging at 1500^{o} C caused the fine 0.02 μm tetragonal precipitates to grow into plates about 0.10 by 0.50 μm. A peak hardness of 1517 kg/mm^2 was obtained after 250 minutes. On further aging monoclinic percipitates formed along grain boundaries. The fracture toughness of the aged and unaged solution-annealed-and-quenched PSZ was found to be between 2 and 3 MN/m$^{3/2}$. This range of fracture toughness is consistent with PSZ's that do not undergo transformation toughening.

17. Key Words (Suggested by Author(s))	18. Distribution Statement
Ceramics Burner rigs Hot corrosions Coatings Thermal barriers	Unclasified - unlimited STAR Category 26

19. Security Classif. (of this report)	20. Security Classif. (of this page)	21. No. of Pages	22. Price*
Unclassified	Unclassified	45	A03

* For sale by the National Technical Information Service, Springfield, Virginia 22161

End of Document